Enhanced Detection of Bubble Emissions Through the Intact Spine for Monitoring Ultrasound-Mediated Blood-Spinal Cord Barrier Opening

Stecia-Marie P. Fletcher, *Student Member, IEEE*, Natalia Ogrodnik, and Meaghan A. O'Reilly, *Member, IEEE*

Abstract*—*Objective: **We previously developed short burst, phase keying (SBPK) focused ultrasound (FUS) to mitigate standing waves in the human vertebral canal. Here, we show microbubble emissions from these pulses can be detected through the human vertebral arch and that these pulses are effective for blood-spinal cord barrier (BSCB) opening.** ***Methods:*** **At $f_0 = 514$ kHz, circulating microbubbles were sonicated through *ex vivo* human vertebrae (60 kPa-1 MPa) using a dual-aperture approach and SBPK exposures engineered to incorporate pulse inversion (PI). Signals from a 250 kHz receiver were analyzed using PI, short-time Fourier analysis and the maximum projection over the pulse train. In rats ($n = 14$), SBPK FUS+microbubbles was applied to 3 locations/spinal cord at fixed pressures ($\sim$0.20–0.47 MPa). MRI and histology were used to assess opening and tissue damage.** ***Results:*** **In human vertebrae between 0.2–0.4 MPa, PI amplified the microbubble/baseline ratio at $f_0/2$ and $2f_0$ by 202 $\pm$ 40% (132–291%). This was maximal at 0.4 MPa, coinciding with the onset of broadband emissions.** ***In vivo*****, opening was achieved at 40/42 locations, with mean MRI enhancement of 46 $\pm$ 32%(16%–178%). Using PI, $f_0/2$ was detected at 14/40 opening locations. At the highest pressures ($f_0/2$ present) histology showed widespread bleeding throughout the focal region. At the lowest pressures, opening was achieved without bleeding.** ***Conclusion:*** **This study confirmed that PI can increase sensitivity to transvertebral detection of microbubble signals. Preliminary *in vivo* investigations show that SBPK FUS can increase BSCB permeability without tissue damage.** ***Significance:*** **SBPK is a clinically relevant pulse scheme and, in combination with PI, provides a means of mediating and monitoring BSCB opening noninvasively.**

***Index Terms*—Focused ultrasound, blood-spinal cord barrier, short bursts, pulse inversion, microbubbles.**

I. Introduction

FOCUSED ultrasound (FUS), in conjunction with circulating microbubbles (MBs), has the potential to transform drug delivery to the central nervous system (CNS) by providing a noninvasive and targeted means of transiently enhancing the permeability of CNS vasculature [1], [2]. Hundreds of preclinical studies using FUS+MBs have reported successful modification of the blood-brain barrier (BBB) and enhanced targeted delivery of a wide range of tracers and therapeutic agents [3]–[12] into the brain parenchyma. FUS-induced BBB opening (BBBO) has reached the stage of clinical trials for the delivery of doxorubicin to brain tumors [13] and for treatment of early to moderate Alzheimer's disease [14]. In the spinal cord, there exists the blood-spinal cord barrier (BSCB) which is functionally and morphologically similar to the BBB [15]. Recently, the application of FUS+MBs for BSCB opening (BSCBO) has shown promising results in preclinical studies [16]–[19].

The safe implementation of microbubble and FUS-induced therapies, like BBBO and BSCBO, hinges on the ability to monitor acoustic emissions from MBs to assess treatment effects. For FUS sonications with quasi-continuous pulses, on the order of milliseconds, the relationship between spectral content of MB emissions and treatment bioeffects have been well characterized [20], [21]. Spectral signatures representing stable MB oscillations, like harmonic emissions, have been associated with BBBO, while spectral signatures indicating inertial cavitation and MB collapse, like broadband noise, have been associated with gross tissue damage. This understanding of the correlation between spectral signatures and tissue effects has been essential for researchers to develop algorithms and controllers based on MB emissions to promote safe BBBO while minimizing tissue damage in real time [22]–[25].

Despite the success of preliminary *in vivo* demonstrations of FUS-induced BSCBO in small animals, delivering and detecting acoustic signals through the complex bony structures of

Manuscript received May 31, 2019; revised July 26, 2019; accepted August 18, 2019. Date of publication August 22, 2019; date of current version April 21, 2020. This work was supported in part by the U.S. National Institute of Biomedical Imaging and Bioengineering under Grant R21EB023996, in part by the Ontario Ministry of Research, in part by Innovation and Science Early Researcher Award (ER17-13-159), and in part by Canada Research Chair Program. *(Corresponding author: Stecia-Marie P. Fletcher.)*

S.-M. P. Fletcher is with Physical Sciences Platform, Sunnybrook Research Institute, Toronto, ON M4N 3M5, Canada, and also with the Department of Medical Biophysics, University of Toronto, Toronto, ON M5G 1L7, Canada (e-mail: sfletcher@sri.utoronto.ca).

N. Ogrodnik is with Physical Sciences Platform, Sunnybrook Research Institute.

M. A. O'Reilly is with Physical Sciences Platform, Sunnybrook Research Institute, and also with the Department of Medical Biophysics, University of Toronto.

Digital Object Identifier 10.1109/TBME.2019.2936972

the human spine remains a challenge that must be overcome for clinical translation. Due to the thickness and density of vertebral bone, FUS delivery through the human spine is subject to focal distortions and low levels of transmission. Using a 514 kHz, single element transducer, a mean FUS transmission of $(31 \pm 17)\%$ of the focal pressure has been reported through posterior elements of *ex vivo* human thoracic vertebrae [26]. To overcome this, phased arrays can be used to correct for phase and amplitude aberrations as FUS propagates through vertebral bone, restoring focal shape and maximizing the focal pressures [27]. Another challenge that arises is the formation of standing waves within the spinal cavity due to reflections off interior walls and the comparatively large focal sizes at submegahertz frequencies. To overcome the challenge posed by standing waves, a dual aperture, cross-beam approach, using short burst, phase keying (SBPK) exposures has been proposed [28]. However, the acoustic emissions from MBs exposed to SBPK exposures are complex and require more advanced methods of analysis compared with conventional exposures. Additionally, small signal contributions from MBs within the vertebral canal may be difficult to identify in the presence of strong reflections at the bone interface, particularly when using short, broadband pulses that overlap the receive bands of interest, giving rise to low contrast-to-tissue ratios [29].

One well established technique to minimize linear tissue signals and amplify non-linear MB signals is pulse inversion (PI). PI was originally developed for ultrasound contrast enhanced imaging by summing reflections from consecutive inverted pulses [29]. This technique has typically not been used in ultrasound therapy because pulses are long compared with imaging pulses, but there have been some demonstrations of BBBO using short pulse lengths [30]–[33]. In such applications, PI could be useful for treatment monitoring and control. Recently PI has been shown to enhance passive imaging of MB activity during ultrasound therapy exposures for BBBO [34].

In this body of work, we demonstrate transvertebral detection of MB emissions from SBPK emissions and identify methods of analysis, including the incorporation of PI to increase detection sensitivity through *ex vivo* human vertebrae. We also perform a preliminary demonstration of BSCBO using SBPK FUS in rats under magnetic resonance imaging (MRI) guidance. During *in vivo* experiments, we capture acoustic signals from MBs and we demonstrate that we can distinguish spectral signatures using the methods of analysis developed on the bench in a less controlled, *in vivo* setting. The implications of these results are then discussed.

II. Methods

A. Short Burst, Phase Keying Pulse Trains With Phase Inversion

SBPK pulse trains were used for FUS delivery in this work, both for delivery through intact *ex vivo* human thoracic vertebrae and *in vivo* to demonstrate efficacy for BSCBO in rats. SBPK pulse trains contain short (2-cycle) bursts with a burst repetition period of 50 μs (burst repetition frequency = 20 kHz). At the start of each burst, a quadrature phase is randomly assigned (0°, 90°, 180° or 270°) as shown in Fig. 1(a). These pulse trains were originally introduced for mitigating standing waves while producing a uniform focus within *ex vivo* human thoracic vertebrae using a dual aperture, cross-beam approach [28]. The short burst length is required to minimize the interference between incident and reflected waves in the vertebral canal, thereby eliminating standing waves [30]. Prior research has shown that a dual aperture, cross-beam approach can reduce the focal size for precise targeting within small cavities by exploiting the region of overlap between ultrasound beams [35]. However, this approach requires a frequency offset between the transducers to avoid banding due to interference patterns at the focus and achieve temporal smoothing. For very short burst lengths, on the order of the short bursts proposed for this work, the frequency offset needed to achieve this is extremely large [28]. To compensate for this, SBPK pulse trains use random phase keying to randomly disrupt interference patterns between incident beams and achieve spatial uniformity over the length of the pulse train.

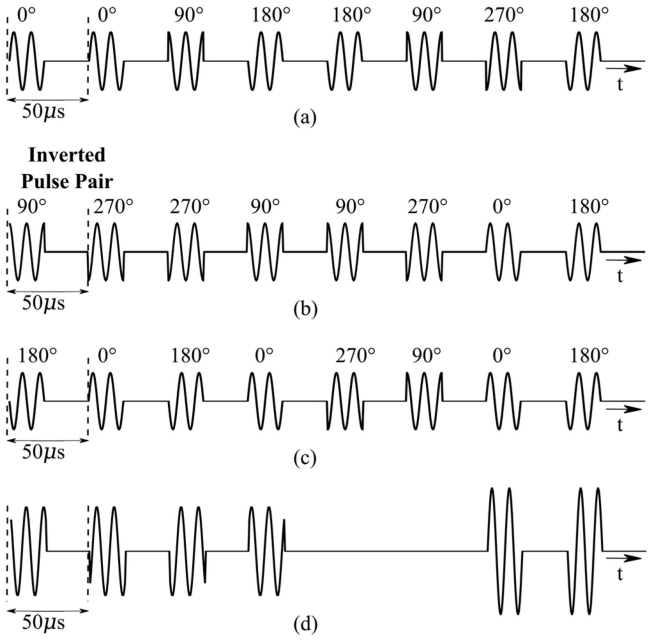

Fig. 1. Truncated examples of (a) a short burst, phase keying pulse train; (b) a short burst, phase keying pulse incorporating pulse inversion used to excite transducer A (Fig. 2(b)); (c) a short burst, phase keying incorporating pulse inversion used to excite transducer B. (Fig. 2(b)). (d) An idealized example of the combined pulse from both transducers at the focus.

In this study, pseudo-random SBPK pulse trains have been engineered to leverage PI to assess its effect on detection of MB emissions through *ex vivo* human vertebrae. To achieve this phase of bursts 1, 3, 5 . . . were randomly assigned, while the phase of bursts 2, 4, 6 . . . were chosen to be 180° shifted from the previous burst. Examples of SBPK pulse trains incorporating PI are shown in Fig. 1(b)&(c). Using a dual aperture, cross-beam approach, the resultant pulse train experienced at the focus due to overlapping beams from transducers excited with the pulse trains described should also result in phase inverted pulse pairs (Fig. 1(d)).

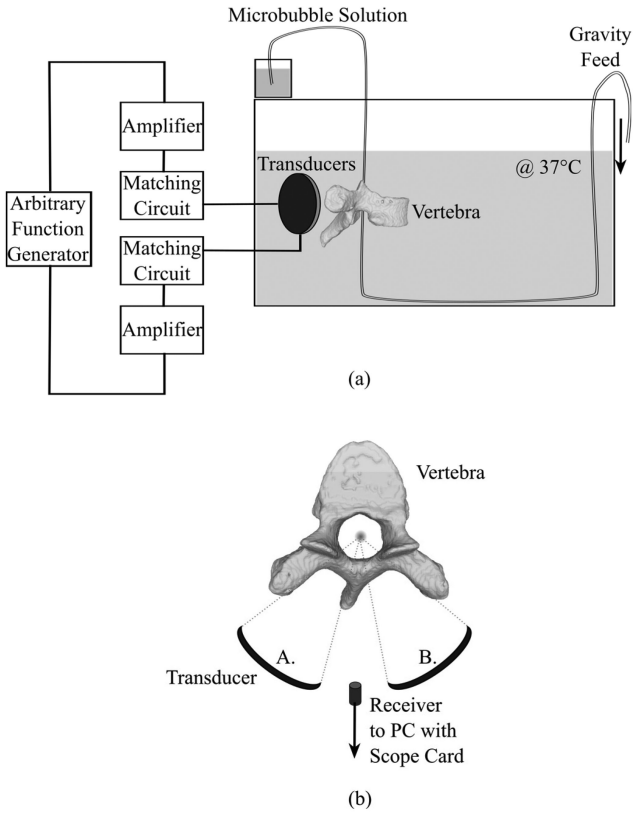

Fig. 2. (a) Schematic diagram showing the experimental set up for exciting microbubbles through intact *ex vivo* human thoracic vertebrae on the benchtop. (b) Schematic diagram showing positions of transducers (A.&B.) and the acoustic receiver with respect to the *ex vivo* vertebra.

B. Benchtop Experiments – Experimental Procedure

The benchtop experimental set up is shown in Fig. 2. To investigate the response of MBs to SBPK FUS exposures, experiments were performed in a tank of degassed, deionized water at 37°C. FUS was generated using two in-house assembled, spherically focused, confocal transducers (elements sourced from DeL Piezo Specialties, LLC, FL, USA) with center frequency, $f_0 = 514$ kHz and F-number 1.2 and an angular separation of 60° (70% focal length ~5.5 mm, focal width ~3.0 mm [28]). Transducers were matched to 50 Ω using an external matching circuit and driven using a dual-channel arbitrary/function generator (AFG 3052C, Tektronix, Beaverton, OR, USA) and 53-dB RF power amplifiers (MP-2519, NP Technologies Inc., Markham, ON, Canada).

2 ms SBPK pulse trains as described in A. (Fig. 1(b)&(c)) were generated in MATLAB and uploaded to the arbitrary/function generator. Different pulse trains were used for each transducer. Each pulse train consisted of 40 bursts in total. (Pulse train duty cycle = 8.4%)

The focus of the transducers was determined by measuring time-domain acoustic field data using a 0.5 mm polyvinylidene difluoride (PVDF) needle hydrophone (Precision Acoustics, Dorchester, UK). The hydrophone was navigated using a 3-D positioning system (Velmex Inc., Bloomfield, NY, USA). Time-domain data from the hydrophone were displayed on a mixed-domain oscilloscope (MDO 3014, Tektronix, Beaverton, OR, USA) and subsequently transferred to a PC, where it was stored and saved. The data were processed in MATLAB to visualize the temporal peak pressure distribution for the ultrasound field and the location at which the maximal pressure was measured was used to determine the focus.

An in-house fabricated, unfocussed, 5 mm diameter lead zirconate titanate (PZT) receiver (element sourced from DeL Piezo Specialties, LLC, FL, USA) with a center frequency of 250 kHz (near the subharmonic, $f_0/2$) was roughly aligned with the focus of the transducers and used to receive acoustic emissions. A 125 MS/s, 14-bit, Peripheral Component Interconnect digitizer (ATS460, Alazar Technologies Inc., Pointe-Claire, QC, Canada) was used to capture receiver signals at a sampling rate of 50 MS/s and data were processed in MATLAB.

A tube phantom with inner diameter = 1.0 mm and wall thickness = 0.3 mm was used to accommodate circulating MBs and was aligned with the focus (Fig. 2(a)). Baseline and MB acoustic signals measurements were performed at increasing peak negative pressures (PNP) between 60 kPa and 1 MPa. Baseline measurements were performed using flowing deionized (not degassed) water. MB measurements were performed using a 1:5000 solution of MBs in deionized water (Definity, Lantheus Medical Imaging, North Billerica, MA, USA), gravity fed through the tubing. The measured flow rate was 0.3 ml/s. Measurements were performed with and without intervening *ex vivo* human thoracic vertebrae (T1, T6, T12). Vertebrae were degassed in a vacuum jar over several days to remove trapped gas, and for a minimum of 2 hours immediately prior to experiments. Once immersed in the water tank, the vertebrae were allowed to sit for 1 hour before measurements were made to allow for thermal equilibrium at 37 °C.

To confirm that results were independent of the receiver bandwidth, an additional set of experiments was performed with T12 on the bench using a 5 mm broadband PVDF receiver [36].

C. BSCBO Using SBPK In Vivo

All animal experiments were approved by the Sunnybrook Research Institute animal care committee and were performed in keeping with guidelines from the Canadian Council on Animal Care. Fourteen (14) Sprague-Dawley rats (male, n = 7, 236–314 g; female, n = 7, 173–268 g; Charles River Laboratories, MA, USA) were anesthetized using 2% isoflurane and oxygen. Prior to the ultrasound exposures the carrier gas was switched to medical air [37], [38]. The hair on their backs was removed using an electric razor, followed by depilatory cream. Ultrasound gel and a water pack were used to acoustically couple the animals to the ultrasound treatment platform. The transducer and receiver set up, described as part of the benchtop experimental procedure, was mounted on a 3-axis positioning arm contained in the water bath of a small animal ultrasound treatment platform (RK-100, FUS Instruments, Toronto, ON). Animals were placed supine on the FUS delivery system. Under MRI-guidance, spinal cords were sonicated using SBPK FUS (10 ms pulse trains comprised of 2-cycle burst at 50 μs intervals; 1 Hz pulse repetition frequency), at 3 locations per spinal cord

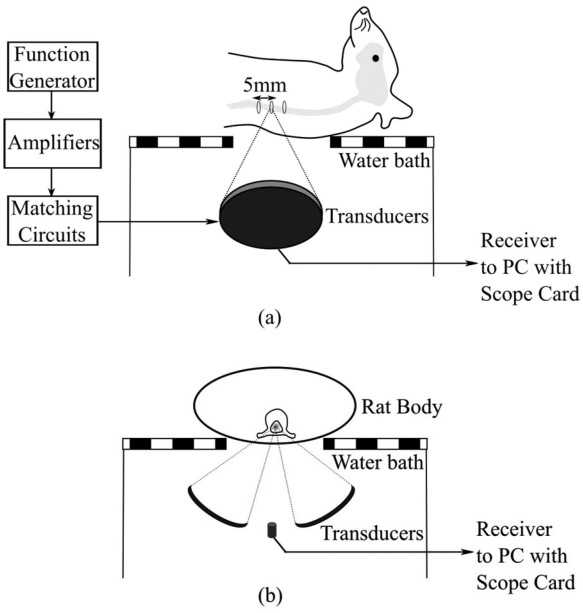

Fig. 3. (a) Schematic diagram showing a transverse view of the experimental set up for *in vivo* experiments. (b) Schematic diagram showing an axial view of the experimental set up for *in vivo* experiments.

TABLE I
ANIMAL DISTRIBUTION FOR *In Vivo* EXPERIMENTS

Treatment duration (minutes)	*In situ* pressure estimate (MPa)	Number of animals
2	0.27	2
	0.34	2
	0.40	2
	0.47	1
5	0.20	3
	0.23	3
	0.27	1

(5 mm spacing), at fixed pressures. MBs (0.02 ml/kg Definity, Lantheus Medical Imaging, MA, USA) were administered intravenously through the tail vein at the start of the sonication. Exposures were interleaved so that all three targets were treated during a single sonication. Fig. 3 shows a diagram of the experimental set up for *in vivo* experiments.

Animals were treated in 2 groups. These groups were treated for different total treatment durations (2 minutes or 5 minutes) at fixed pressures. Treatment parameters are outlined in Table I. *In situ* pressure estimates were based on a mean pressure transmission of 67 $\pm$ 15% through the rat spine at 551.5 kHz reported in [18]. Acoustic signals were acquired during treatments using the same digitizer as the *ex vivo* experiments, and were analyzed using the methods developed on the bench. The narrowband PZT receiver was used as the PVDF receiver was not available at the time of these experiments.

BSCBO was confirmed using coronal, T1-weighted, contrast enhanced magnetic resonance imaging (MRI) (0.2 ml/kg gadolinium, Field of view = 4 cm $\times$ 4 cm, Spatial discretization = 200 μm, Slice thickness = 1 mm, Echo time = 5.3 ms, Repetition time = 500 ms, Rare factor = 4, Number of averages = 6; Biospec 7T, Bruker Co., MA, USA). Post-treatment, intravenously administered Evan's blue (EB) dye (2.5 ml/kg) was used to verify opening and locate treatment locations after tissue harvesting. BSCBO was considered successful if the mean MRI signal in a 3 $\times$ 3 voxel area centered on maximum enhancement was at least 2 standard deviations greater than the mean signal in a baseline 3 $\times$ 3 voxel unsonicated area in the spinal cord. MRI images were analyzed using Medical Image Processing, Analysis and Visualization (MIPAV; National Institutes of Health, Bethesda, MD, USA). 2 hours post-treatment, spinal cords were formalin fixed through transcardial perfusion under deep anesthetic and harvested for histological staining. 5 μm thick coronal sections at 100 μm intervals were stained using hematoxylin and eosin (H&E) and evaluated for tissue damage.

TABLE II
HISTOLOGY GRADES

Grade	Description
0	No damage on all histology levels
1	Very minor damage – 1 to a few very small clusters of red blood cells on at least 1 histology level
2	Moderate (more significant) damage – 1 larger cluster of red blood cells or a greater number of small clusters of red blood cells on at least 1 histology level
3	Extensive damage – A large number of clusters of red blood cell extravasation, with or without pooling on at least 1 histology level.

Tissue damage at each treatment location was evaluated using a 4 point grading scheme adapted from [39] as described in Table II. Two researchers independently graded the histology and were blinded to treatment parameters, results of BSCBO and results of the acoustic monitoring.

III. RESULTS

A. Benchtop Experiments

Fig. 4(a) and (b) show examples of time-domain signals measured for a baseline case and a MB case respectively at the posterior surface of T6 at PNP = 0.26 MPa. The results of performing Fourier transforms on these data are shown in Fig. 4(c) and (d). These frequency spectra are normalized to the maximum for the baseline case. The spectra shown in Fig. 4(c) and (d) are complicated by peaks at intervals of the pulse repetition frequency of the bursts within the pulse train (20 kHz). To overcome this, 35 μs windows, 50 μs apart, containing the received signals from a single burst were analyzed. (A truncated window length of 35 μs was chosen for benchtop experiments as it maximized sensitivity to detecting spectral content.) Following Fourier analysis, maps of how frequency content evolved throughout the pulse train (burst number) were plotted for the baseline (Fig. 4(e)) and MB cases (Fig. 4(f)).

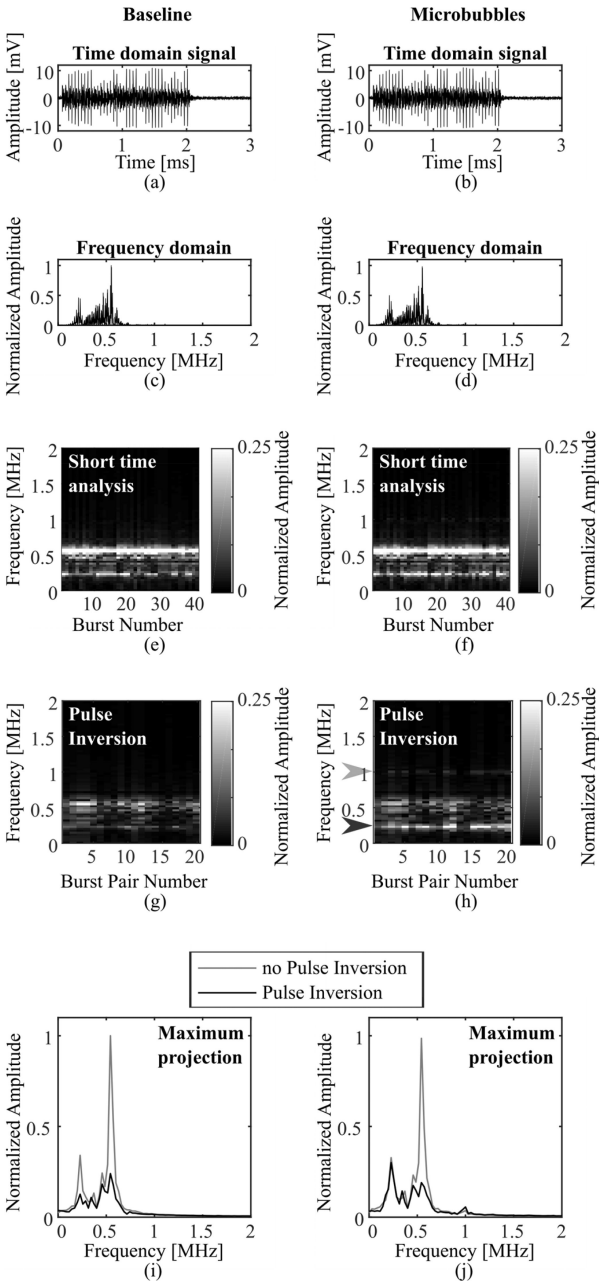

Fig. 4. Examples of baseline (a) and microbubble (b) time domain signals measured by the receiver, and their corresponding frequency spectra (c,d). Corresponding spectrograms without (e, f) and with (g, h) pulse inversion are shown. In (h), the dark gray arrow shows $f_0/2$, while the light gray arrow shows $2f_0$. (i, j) Show the maximum projections of (e,h) and (f,h) respectively across all burst pairs.

To determine the effect of PI, consecutive time-domain windows were added before Fourier analysis. The resulting maps of frequency against burst pair are shown in Fig. 4(g) and (h) for the baseline and MB case respectively.

The different bursts in the SBPK pulse train inherently have different pressure, due to the changing interference pattern of the ultrasound from the two apertures. A maximum projection of frequency content of the entire pulse train was used to improve sensitivity to temporally short events (i.e., identifying events even if they occur during only a single burst). For the example in Fig. 4, these projections are shown in Fig. 4(i) and (j) for baseline and MB cases respectively, both with and without PI.

The effect of PI was most obvious around the center frequency of the receiver ($f_0/2$). In the baseline case (Fig. 4(i)) the signal at the fundamental and the subharmonic are reduced by 76% and 63% respectively, in this example. The reduction observed at the center frequency ($f_0/2$) is likely linked to the reduction of the broadband fundamental signal. In the MB case, the fundamental and the subharmonic are reduced by 81% and 8% respectively. This indicates improved sensitivity to detecting the subharmonic through quantifying the MB/baseline ratio. In the MB case, the signal at the 2nd harmonic, $2f_0$, increased by 56%.

The simultaneous reduction in baseline signal and increase in MB signal led to the hypothesis that the effect of PI could be well characterized by considering the ratio in spectral amplitude between MB signal and baseline signal. Fig. 5(a)–(c) show mean MB/baseline ratios without intervening vertebrae and Fig. 5(d)–(i) show mean MB/baseline ratios with intervening *ex vivo* thoracic vertebrae (T1:(d) and (e), T6: (f) and (g), T12: (h) and (i)). (Error bars represent the standard deviation over 10 measurements.) MB/baseline ratios were calculated using the area under the spectra in the range 0.25 ± 0.10 MHz for $f_0/2$ and 0.97 ± 0.10 MHz for $2f_0$. Fig. 5(a) shows the MB/baseline ratio at $f_0/2$ for increasing focal PNPs in water. In the pressure range 0.2–0.4 MPa, the amplification of the MB/baseline ratio at $f_0/2$ was $145 \pm 24\%$ (minimum: 120%, maximum: 175%). In the same pressure range, the amplification of the MB/baseline ratio at $2f_0$ was $158 \pm 12\%$ (minimum:144%, maximum:172%) (Fig. 5(b)). Broadband noise was measured in the range 1.70 ± 0.10 MHz, far away from the receiver center frequency and where the investigators did not observe detected harmonic spectral content. The measured onset of inertial cavitation was at 0.4 MPa. Above this threshold, the MB/baseline ratio did not increase with PNP (with and without PI). The MB/baseline ratio amplification resulting from PI at $f_0/2$ decreased from a maximum of 175% at 0.40 MPa to a minimum of 144% in the inertial cavitation regime.

Across the 3 vertebrae, in the range 0.2-0.4 MPa, the amplification of the MB/baseline ratio at $f_0/2$ was $197 \pm 48\%$ (minimum:132%, maximum: 291%). The amplification of the MB/baseline ratio at the $2f_0$ in the same range was $207 \pm 31\%$ (minimum: 150%, maximum: 250%). Above 0.4 MPa (threshold for inertial cavitation measured in water), the MB/baseline ratio no longer increased, but dropped off quickly, both with and without PI. Above 0.7 MPa, small signals at $f_0/2$ could not be detected even with PI.

Using the broadband receiver, in the range 0.2-0.4 MPa, the amplification of the MB/baseline ratio at $f_0/2$ through T12 was $153 \pm 11\%$ (minimum: 142%, maximum: 167%). The amplification of the MB/baseline ratio at the $2f_0$ in the same range was $376 \pm 77\%$ (minimum: 290%, maximum: 470%). Above 0.4 MPa, the MB/baseline ratio plateaued.

B. In Vivo Experiments

MRI enhancement values indicated successful BSCBO at 40/42 treatment locations (Enhancement: $52 \pm 41\%$ (2 min;

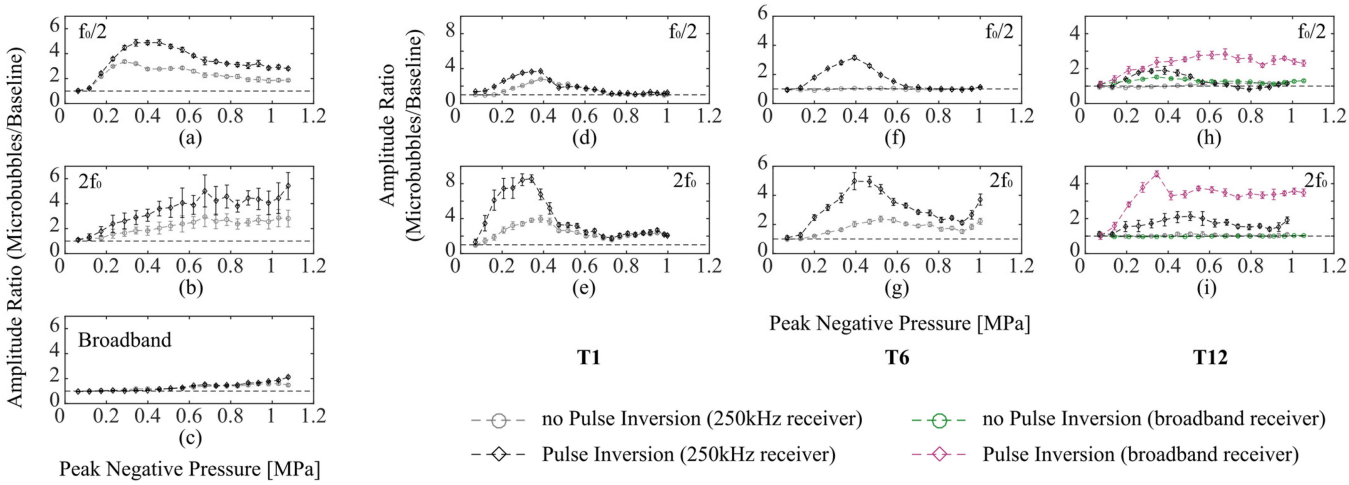

Fig. 5. Microbubble to baseline ratios for different focal pressures in water (a-c), through T1 (d, e), T6 (f, g) and T12 (h, i). PI is shown to increase detection sensitivity at the $f_0/2$ (a, d, f, h) and $2f_0$ (b, e, g, i) in water and through all measured vertebrae. In water, the onset of inertial cavitation was detected around 0.4 MPa (c) and is thought to be responsible for the decrease in $f_0/2$ and $2f_0$ emissions at high exposures as energy is redistributed to the inertial bands.

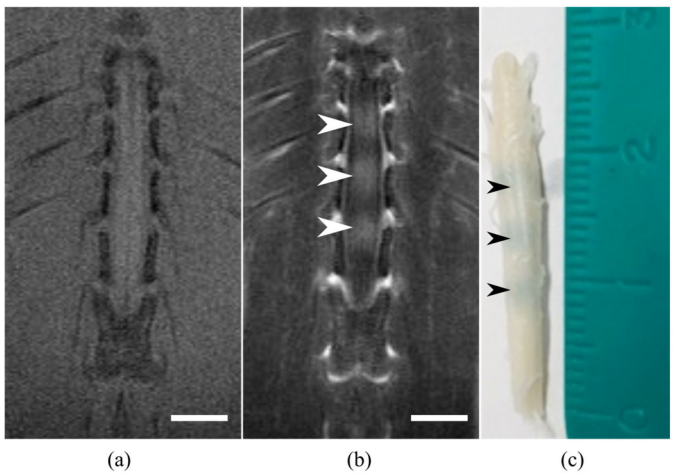

Fig. 6. (a) Pre-treatment T1-weighted MRI of the rat spine. (b) Post-treatment, contrast-enhance T1-weighted MRI of the rat spine after sonication with short burst, phase keying focused ultrasound at 0.23 MPa for five minutes. This image shows contrast enhancement at three locations in the spinal cord. (c) Perfused spine of the animal shown in (d) showing Evan's Blue enhancement at three locations. Scalebar = 5 mm.

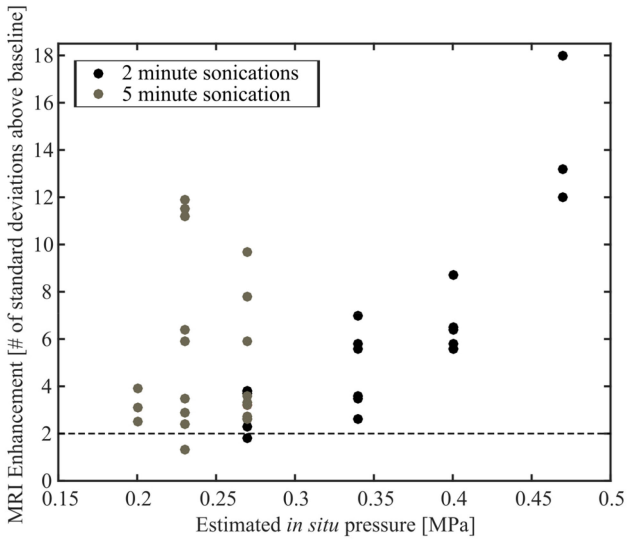

Fig. 7. Scatter plots showing the relationship between estimated *in situ* pressure and MRI enhancement in units of number of standard deviations above baseline for two minute and five minute sonications.

minimum: 16%, maximum: 178%); 41 ± 22% (5 min; minimum: 16%, maximum: 85%)). An example of a T1-weighted MRI of the rat spinal cord is shown in Fig. 6(a). A post-treatment (pressure: 0.23 MPa, duration: 5 min) contrast-enhanced MRI of the same spinal cord is shown in Fig. 6(b). Opening was confirmed using EB staining (Fig. 6(c)). Fig. 7 shows the relationship between estimated *in situ* pressure and MRI enhancement expressed as number of standard deviations above baseline.

Representative images of histology grades are shown in Fig. 8. A summary of assigned histology grades is given in Table III. Of the 2 treatment locations where BSCBO was not confirmed using MRI enhancement, 1 was assigned a Grade 0 and 1 was assigned a Grade 1. The later was considered borderline during analysis of MRI signal enhancement, with a signal increase of 1.8 standard deviations compared with baseline.

Using the methods developed on the bench and a window length of 50 μs for short time analysis, the maximum projection of the acquired frequency spectra over the total treatment duration compared to baseline measurements were visualized. Fig. 9 shows representative images of acquired acoustic emissions spectra in 3 cases: (a) BSCB open with $f_0/2$ and $2f_0$ present, (b) BSCB open with only $2f_0$ present, and (c) BSCB closed with no spectral signals visible. A peak at $f_0/2$ was qualitatively distinguishable above baseline noise for 14/40 treatment locations where BSCBO was confirmed using MRI enhancement. 13 of these locations were during 2 minute sonications

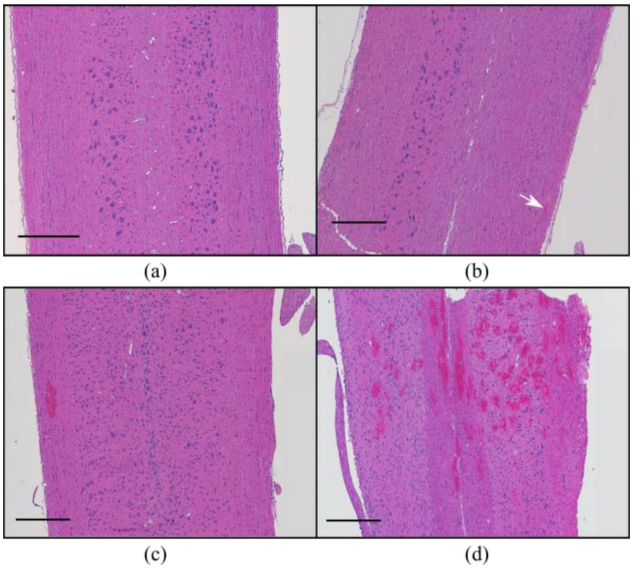

Fig. 8. Representative histology images of different damage levels: (a) Grade 0, (b) Grade 1 (white arrow shows red blood cell extravasation), (c) Grade 2, (d) Grade 3. Scale bar = 0.5 mm.

TABLE III
ASSIGNED HISTOLOGY GRADES

Grade	Number of treatment locations (total =41[a])	Pressure range min-max (MPa)
0	2	0.23
1	13	0.20-0.27
2	12	0.23-0.34
3	12	0.34-0.47

[a] 1 treatment location with opening confirmed by MRI enhancement was excluded from scoring due to a cutting artifact at that location resulting from processing for histology.

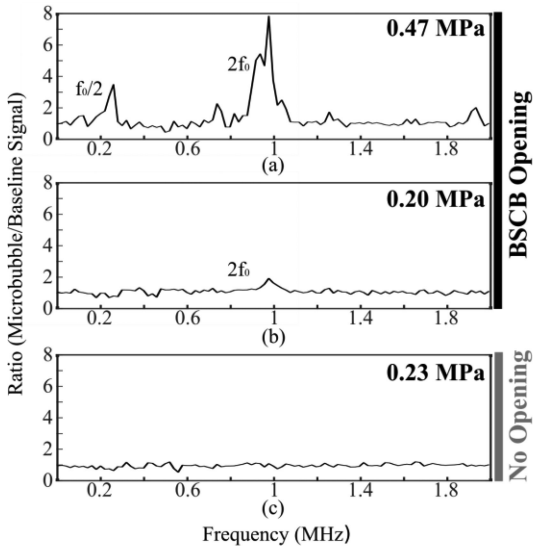

Fig. 9. Example of frequency spectra with: (a) Subharmonic and 2nd harmonic visible (0.47 MPa, BSCB open), (b) only 2nd harmonic visible (0.20 MPa, BSCB open), (c) no spectral signatures visible (0.23 MPa, BSCB closed).

TABLE IV
RELATIONSHIP BETWEEN BSCBO AND ACOUSTIC EMISSIONS

	$f_0/2$ observed (number/total)	$2f_0$ observed (number/total)
Open	14/40	38/40
Not open	0/2	0/2

TABLE V
RELATIONSHIP BETWEEN HISTOLOGY GRADES AND ACOUSTIC EMISSIONS

Grade	$f_0/2$ observed (number/total)	$2f_0$ observed (number/total)
0	0/2	0/2
1	1/13	13/13
2	4/12	12/12
3	9/12	12/12

[a] 1 treatment location with opening confirmed by MRI enhancement was excluded from scoring due to a cutting artifact at that location resulting from processing for histology. $f_0/2$ was not observed at this location.

(0.34-0.47 MPa) and 1 of these locations was during a 5 minute sonication (0.23 MPa). A peak at the $2f_0$ was distinguishable above baseline at 38/40 treatment locations where BSCBO was confirmed using MRI signal enhancement. The $2f_0$ peak was absent at 2 locations (0.23 MPa, 5 min sonications). At the 2 treatment locations where BSCBO was not confirmed, neither the 2nd harmonic nor the subharmonic was observed. These results are summarized in Table IV.

Table V summarizes the relationship between histology grades and observations of acoustic emissions at $f_0/2$ and $2f_0$ at locations with successful BSCBO. $2f_0$ was not observed at the 2 points assigned Grade 0. However, it was observed at 100% of the points assigned a higher grade where BSCBO was observed. The percentage of treatment locations at which $f_0/2$ was observed increased for higher histology grades.

IV. DISCUSSION

In this paper, we have proposed a method of analysis for enhancing the detection of microbubble emissions through the intact human spine during SBPK FUS exposures. This method involves dividing received signals from pulse trains into short time windows and implementing PI to amplify nonlinear signals emitted by microbubbles. Further, as the bursts in SBPK pulse trains inherently have different pressure magnitudes due to the interference between phase shifted pulses from the two transducers, we have proposed the use of a maximum projection across each pulse train to best capture acoustic events. Additionally, using a maximum projection increases the sensitivity to detecting temporally limited events that could be averaged out if using a mean projection [40].

A comparison between analysis with and without PI showed that PI yielded amplification of both the sub and second harmonic signals below the threshold for inertial cavitation. PI has been well established as a means of enhancing MB signals in ultrasound imaging [29] and has recently been shown to enhance

passive acoustic mapping during ultrasound therapy exposures *in vitro* and *in vivo* in small animals [34]. Here, we demonstrate that PI can be easily integrated with SBPK exposures to enhance the detection of acoustic signatures through the human vertebral arch. SBPK with PI is a pulse scheme that is highly relevant to clinical translation as it allows standing wave-free therapeutic exposures without sacrificing cavitation detection ability as a result of the shorter bubble excitations. A consequential observation of this study was that the effect of PI was minimized above the threshold of inertial cavitation, as measured in free field, perhaps limiting the potential of this method for applications other than BSCBO, where higher exposures might be of interest.

In vivo, we demonstrated BSCBO using SBPK FUS in a small cohort of rats (n = 14). Through comparing acoustic signals analyzed using the method developed on the bench and tissue histology, the subharmonic was shown to be more likely for higher levels of treatment damage, which is consistent with studies at longer burst lengths.

Based on the current study, the 2nd harmonic was shown to be a reliable indicator of BSCBO, despite low receiver sensitivity in that band. It was present in 95% where opening was seen on MRI and it was absent in all cases where no opening was observed. The proportion of treatment locations at which the subharmonic was observed increased for higher histological damage scores, which is promising for its use as a predictor of tissue damage. However, at the highest level of tissue damage, the subharmonic was only observed at 75% of treatment locations. The authors believe that the high rate of false negatives could be attributed to some study limitations that are discussed later in this section.

The limitations of this study include the small sample size for *in vivo* experiments, single timepoint of tissue harvesting and the use of a small, single element, narrowband receiver. Not only did this study use a small total number of animals, but a very small number were used at each exposure level. It has previously been reported [18] that the *in situ* pressures in the rat spinal canal vary strongly with location, therefore the true pressures likely vary to a strong degree. In the absence of active treatment control, we distributed the animals in this preliminary study to capture a range of observed bioeffects and acoustic signals. Due to the small sample size, it is difficult to draw conclusions regarding the correlation of the second harmonic and subharmonic emissions with BSCBO and tissue damage. However, the data collected in these experiments indicate that the detection of these emissions may be a relevant metric for treatment monitoring during BSCBO with SBPK + FUS and further investigation in a larger cohort of animals is warranted, but is beyond the scope of the present study. Since this is an acute study, all tissues were harvested for histology $\sim$2 hours after treatment. Previous work has shown that even when edema and RBC extravasation are evident immediately following the treatment, these effects could be resolved at later timepoints [22]. It would be useful to investigate whether the treatment parameters which resulted in Grade 1 scores during histological analysis would still yield observable tissue damage after 24 hours or several days.

For this study, no sham animals (sonicated in the absence of microbubbles) were tested, however baseline acoustic emissions without microbubbles were captured, but without associated MR images to confirm effect on the BSCB. It is known that pulsed focused ultrasound, in the absence of intravenously injected microbubbles, can modify the blood-brain barrier. However, it has been shown that this effect is associated with the presence of subharmonic emissions [41] which were not observed in our baseline measurements. Previous work that included sham animals, showed minimal increase in blood-brain barrier permeability in the absence of bubbles [1] at pressures an order of magnitude higher than those used in this study (5 MPa vs 0.47 MPa in this study). Future studies might benefit from including shams for histological comparison.

In future work, the use of a wideband PVDF receiver [36], or multiple narrowband receivers with different center frequencies, may improve the detection of multiple frequency bands *in vivo*. The receiver used in this study was centered at the subharmonic (250 kHz) to optimize sensitivity to the subharmonic emissions. As the vertebral bone attenuates higher frequency signals to a greater degree, we chose to focus on detecting signals that would be better transmitted through the bone and that have been associated with tissue damage. Although the subharmonic was the main frequency of interest, the choice of receiver compromised the quality of results outside of this band, including at the 2nd harmonic (1.03 MHz). Useful data was obtained at the 2nd harmonic, but some acoustic events may not have been detected due to reduced receiver sensitivity. For example, the presence of the 2nd harmonic is expected to be a useful indicator of successful barrier opening [20], but here we observed 2 cases where BSCBO was achieved based on MRI enhancement values, but no 2nd harmonic signal was observed. Both cases occurred for comparatively low *in situ* estimates of pressure (0.23 MPa). The low sensitivity of the receiver at the 2nd harmonic could explain the absence of this signature in these cases. We also note that the additional bench experiments conducted using the PVDF receiver showed excellent sensitivity to both sub and 2nd harmonic signals when combined with PI. While this receiver was not available at the time of the *in vivo* investigations, several PVDF receivers have now been fabricated that will be used in future *in vivo* studies.

Further, this study used a simple experimental configuration with a single element receiver for passive cavitation detection. Such receivers are limited for this purpose because they are unable to provide spatial information about received acoustic signals. This makes them susceptible to inclusion of acoustic events outside of the focal region (E.g. an air bubble in the water bath) or exclusion of relevant acoustic events. Through the intact human skull, phased array receivers have been shown to allow spatial mapping of acoustic signals [42]–[44]. Additionally, this study used a transpinous approach for detecting acoustic emissions, but a translaminar approach would likely increase sensitivity to acoustic events through the human spine. Ideally, before FUS-induced BSCBO treatments reach the stage of clinical application, a receive array can be incorporated with the transmit array designed in [27] to provide robust spatial-temporal acoustic emissions detection for treatment control.

Results from this study indicate the need for several future investigations. Firstly, a larger scale parameter study in a small animal model is required to determine optimum treatment parameters, such as the time between bursts in SBPK pulse trains, pulse train length and treatment duration. Regarding the latter, the results of this study suggest that a 5 min duration achieves superior tracer accumulation across the BSCB compared with a 2 min sonication duration at low pressures. This larger cohort study can also be used to robustly characterize the associations between the cavitation signals and observed bioeffects in order to advance towards implementing actively controlled SBPK treatments. Additionally, the methods proposed here need to be validated in a clinically relevant, large animal model.

V. Conclusion

A method of analyzing and enhancing the detection of acoustic signals from MBs sonicated with SBPK FUS has been proposed. This involves the use of PI, which was shown to increase sensitivity to detecting subharmonic and 2nd harmonic emissions. This method was first tested on the benchtop, using *ex vivo* human vertebrae, and was then utilized for detecting *in vivo* signals at fixed pressure levels in a rat model. Preliminary *in vivo* investigations showed that SBPK FUS exposures can successfully modify the BSCB and that PI improves detection of bubble activity under these exposures. At the lowest pressures investigated, BSCBO was achieved with no or minor tissue damage, typically accompanied by a peak at the 2nd harmonic. At the highest pressures investigated, BSCBO was accompanied by widespread RBC extravasation and hemorrhage. Detection of the subharmonic was shown to be more likely at higher levels of tissue damage, indicating potential use in a future treatment control algorithm. SBPK with PI is a clinically relevant pulse scheme for therapeutic ultrasound exposures of the spinal cord, and this work advances our goal of translating ultrasound-mediated drug delivery to the spinal cord to clinical scale.

Acknowledgment

The authors would like to thank B. Hynynen, C. Nantel, S. Seerala, M. Choi and P. Smith for experimental assistance, and Dr. R. Jones for experimental assistance and general discussion. They would also like to thank D. McMahon for assistance with histology analysis and Dr. H. Lea-Banks for assistance with acoustic signal analysis. Finally, they would like to acknowledge V. Chan for veterinary care and J. Sun for tissue processing for histology.

References

[1] K. Hynynen *et al.*, "Noninvasive MR imaging-guided focal opening of the blood-brain barrier in rabbits," *Radiology*, vol. 220, no. 3, pp. 640–646, 2001.

[2] N. Sheikov *et al.*, "Cellular mechanisms of the blood-brain barrier opening induced by ultrasound in presence of microbubbles," *Ultrasound Med. Biol.*, vol. 30, no. 7, pp. 979–989, 2004.

[3] L. H. Treat *et al.*, "Targeted delivery of doxorubicin to the rat brain at therapeutic levels using MRI-guided focused ultrasound," *Int. J. Cancer*, vol. 121, no. 4, pp. 901–907, 2007.

[4] H.-L. Liu *et al.*, "Blood-brain barrier disruption with focused ultrasound enhances delivery of chemotherapeutic drugs for Glioblastoma treatment," *Radiology*, vol. 255, no. 2, pp. 415–425, 2010.

[5] M. Aryal *et al.*, "Multiple treatments with liposomal doxorubicin and ultrasound- induced disruption of blood-tumor and blood-brain barriers improves outcomes in a rat glioma model," *J. Controlled Release*, vol. 169, pp. 103–111, 2013.

[6] J. F. Jordão *et al.*, "Antibodies targeted to the brain with image-guided focused ultrasound reduces amyloid-β plaque load in the TgCRND8 mouse model of Alzheimer's disease," *PLoS One*, vol. 5, no. 5, 2010, Art. no. e10549.

[7] M. Kinoshita *et al.*, "Targeted delivery of antibodies through the blood-brain barrier by MRI-guided focused ultrasound," *Biochem. Biophys. Res. Commun.*, vol. 340, no. 4, pp. 1085–1090, 2006.

[8] P.-H. Hsu *et al.*, "Noninvasive and targeted gene delivery into the brain using microbubble-facilitated focused ultrasound," *PLoS One*, vol. 8, no. 2, Feb. 2013, Art. no. e57682.

[9] C.-Y. Lin *et al.*, "Focused ultrasound-induced blood-brain barrier opening for non-viral, non-invasive, and targeted gene delivery," *J. Controlled Release*, vol. 212, pp. 1–9, 2015.

[10] A. Burgess *et al.*, "Targeted delivery of neural stem cells to the brain using MRI-guided focused ultrasound to disrupt the blood- brain barrier," *PLoS One*, vol. 6, no. 11, 2011, Art. no. e27877.

[11] R. Alkins *et al.*, "Early treatment of HER2-amplified brain tumors with targeted NK-92 cells and focused ultrasound improves survival," *Neuro-Oncology*, vol. 18, no. 7, pp. 974–981, 2016.

[12] P.-H. Hsu *et al.*, "Focused ultrasound-induced blood-brain barrier opening enhances GSK-3 inhibitor delivery for amyloid-beta plaque reduction OPEN," *Sci. Rep.*, vol. 8, no. 1, 2018, Art. no. 12882.

[13] T. Mainprize *et al.*, "Blood-brain barrier opening in primary brain tumors with non-invasive MR-guided focused ultrasound: A clinical safety and feasibility study," *Sci. Rep.*, vol. 9, no. 1, 2019, Art. no. 321.

[14] N. Lipsman *et al.*, "Blood-brain barrier opening in Alzheimer's disease using MR-guided focused ultrasound," *Nature Commun.*, vol. 9, no. 1, 2018, Art. no. 2336.

[15] V. Bartanusz *et al.*, "The blood-spinal cord barrier: Morphology and clinical implications," *Ann. Neurol.*, vol. 70, no. 2, pp. 194–206, 2011.

[16] D. Weber-Adrian *et al.*, "Gene delivery to the spinal cord using MRI-guided focused ultrasound," *Gene Therapy*, vol. 22, no. 7, pp. 568–577, 2015.

[17] A. H. Payne *et al.*, "Magnetic resonance imaging-guided focused ultrasound to increase localized blood-spinal cord barrier permeability," *Neural Regenaration Res.*, vol. 12, no. 12, pp. 2045–2049, 2017.

[18] M. A. O'Reilly *et al.*, "Preliminary investigation of focused ultrasound-facilitated drug delivery for the treatment of leptomeningeal metastases," *Sci. Rep.*, vol. 8, no. 9013, pp. 1–8, 2018.

[19] J. Wachsmuth, R. Chopra, and K. Hynynen, "Feasibility of transient image-guided blood-spinal cord barrier disruption," *AIP Conf. Proc.*, vol. 1113, no. 1, pp. 256–259, 2009.

[20] N. McDannold, N. Vykhodtseva, and K. Hynynen, "Targeted disruption of the blood–brain barrier with focused ultrasound: Association with cavitation activity," *Phys. Med. Biol.*, vol. 51, pp. 793–807, 2006.

[21] Y.-S. Tung *et al.*, "In vivo transcranial cavitation threshold detection during ultrasound-induced blood–brain barrier opening in mice," *Phys. Med. Biol.*, vol. 55, pp. 6141–6155, 2010.

[22] M. A. O'Reilly and K. Hynynen, "Blood-brain barrier: Real-time feedback-controlled focused ultrasound disruption by using an acoustic emissions-based controller," *Radiology*, vol. 263, no. 1, pp. 96–106, 2012.

[23] T. Sun *et al.*, "Closed-loop control of targeted ultrasound drug delivery across the blood-brain/tumor barriers in a rat glioma model," *Proc. Nat. Acad. Sci.*, vol. 114, no. 48, pp. E10281–E10290, 2017.

[24] C.-H. Tsai *et al.*, "Real-time monitoring of focused ultrasound blood-brain barrier opening via subharmonic acoustic emission detection: Implementation of confocal dual-frequency piezoelectric transducers," *Phys. Med. Biol.*, vol. 61, 2016, Art. no. 2926.

[25] C. D. Arvanitis *et al.*, "Controlled ultrasound-induced blood-brain barrier disruption using passive acoustic emissions monitoring," *PLoS One*, vol. 7, no. 9, 2012, Art. no. e45783.

[26] R. Xu and M. A. O'Reilly, "Simulating transvertebral ultrasound propagation with a multi-layered ray acoustics model," *Phys. Med. Biol.*, vol. 63, no. 14, 2018, Art. no. 145017.

[27] R. Xu and M. A. O'Reilly, "A spine-specific phased array for transvertebral ultrasound therapy: Design and simulation," *IEEE Trans. Biomed. Eng.*, vol. 67, no. 1, pp. 256–267, Jan. 2020.

[28] S.-M. P. Fletcher and M. A. O'Reilly, "Analysis of multifrequency and phase keying strategies for focusing ultrasound to the human vertebral canal," *IEEE Trans. Ultrason. Ferroelectr. Freq. Control*, vol. 65, no. 12, pp. 2322–2331, Dec. 2018.
[29] D. Hope Simpson, C. Ting Chin, and P. N. Burns, "Pulse inversion doppler: A new method for detecting nonlinear echoes from microbubble contrast agents," *IEEE Trans. Ultrason. Ferroelectr. Freq. Control*, vol. 46, no. 2, pp. 372–382, Mar. 1999.
[30] M. A. O'Reilly, Y. Huang, and K. Hynynen, "The impact of standing wave effects on transcranial focused ultrasound disruption of the blood-brain barrier in a rat model," *Phys. Med. Biol.*, vol. 55, no. 18, pp. 5251–5267, 2010.
[31] M. A. O'Reilly *et al.*, "Focused-ultrasound disruption of the blood-brain barrier using closely-timed short pulses: Influence of sonication parameters and injection rate," *Ultrasound Med. Biol.*, vol. 37, no. 4, pp. 587–594, 2011.
[32] J. J. Choi *et al.*, "Noninvasive and localized neuronal delivery using short ultrasonic pulses and microbubbles," *Proc. Nat. Acad. Sci. U S A*, vol. 108, no. 40, pp. 16539–16544, 2011.
[33] S. V Morse *et al.*, "Rapid short-pulse ultrasound delivers drugs uniformly across the murine blood-brain barrier with negligible disruption," *Radiology*, vol. 291, pp. 459–466, 2019.
[34] A. N. Pouliopoulos, M. T. Burgess, and E. E. Konofagou, "Pulse inversion enhances the passive mapping of microbubble-based ultrasound therapy," *Appl. Phys. Lett*, vol. 113, 2018, Art. no. 44102.
[35] T. Sun *et al.*, "Transcranial cavitation-mediated ultrasound therapy at sub-MHz frequency via temporal interference modulation," *Appl. Phys. Lett.*, vol. 111, no. 163701, pp. 1–4, 2017.
[36] M. A. O'Reilly and K. Hynynen, "A PVDF receiver for ultrasound monitoring of transcranial focused ultrasound therapy," *IEEE Trans. Biomed. Eng.*, vol. 57, no. 9, pp. 2286–2294, Sep. 2010.
[37] N. McDannold, Y. Zhang, and N. Vykhodtseva, "Blood-brain barrier disruption and vascular damage induced by ultrasound bursts combined with microbubbles can be influenced by choice of anesthesia protocol," *Ultrasound Med. Biol.*, vol. 37, no. 8, pp. 1259–1270, 2011.
[38] N. McDannold, Y. Zhang, and N. Vykhodtseva, "The effects of oxygen on ultrasound-induced blood-brain barrier disruption in mice," *Ultrasound Med. Biol.*, vol. 43, no. 2, pp. 469–475, 2017.
[39] K. Hynynen *et al.*, "Local and reversible blood-brain barrier disruption by noninvasive focused ultrasound at frequencies suitable for trans-skull sonications," *NeuroImage*, vol. 24, no. 1, pp. 12–20, 2005.
[40] C. N. Acconcia, R. M. Jones, and K. Hynynen, "Receiver array design for sonothrombolysis treatment monitoring in deep vein thrombosis," *Phys. Med. Biol.*, vol. 63, no. 23, 2018, Art. no. 235017.
[41] N. I. Vykhodtseva, K. Hynynen, and C. Damianou, "Histologic effects of high intensity pulsed ultrasound exposure with subharmonic emission in rabbit brain in vivo," *Ultrasound Med. Biol.*, vol. 21, no. 7, pp. 969–979, 1995.
[42] R. M. Jones, M. A. O'Reilly, and K. Hynynen, "Experimental demonstration of passive acoustic imaging in the human skull cavity using CT-based aberration corrections," *Med. Phys.*, vol. 42, no. 7, pp. 4385–4400, 2015.
[43] R. M. Jones *et al.*, "Three-dimensional transcranial microbubble imaging for guiding volumetric ultrasound-mediated blood-brain barrier opening," *Theranostics*, vol. 8, no. 11, pp. 2909–2926, 2018.
[44] C. D. Arvanitis and N. McDannold, "Integrated ultrasound and magnetic resonance imaging for simultaneous temperature and cavitation monitoring during focused ultrasound therapies," *Med. Phys.*, vol. 40, no. 11, 2013, Art. no. 112901.